DETERMINATION OF THE SINGLE- AND MULTI- PHASE TRANSPORT PROPERTIES OF A LAYERED SOIL BY COMBINING LABORATORY EXPERIMENTS WITH NUMERICAL CALCULATIONS

CHRISTOS D. TSAKIROGLOU, CHRISTOS AGGELOPOULOS

Institute of Chemical Engineering and High Temperature Chemical Processes – Foundation for Research and Technology, Stadiou str., Platani, P.O.Box 1414, GR-26504 Patras, Greece

ABSTRACT

Depending on the texture of the (non-fractured) porous matrix of a layered soil, the single- and multi-phase transport properties are either estimated with history matching of displacement experiments or calculated from microscopic properties of the pore structure. For the permeable sandy layers, immiscible and miscible displacement experiments are performed on disturbed and undisturbed soil columns, and the electrical resistance along the columns is monitored. The electrical measurements are employed to calculate the transient response of the water saturation profile along the column, as well as the solute concentration breakthrough curve at various axial positions of the column. The experimental datasets are introduced into numerical codes of inverse modeling of the two-phase flow and advection-dispersion equations to estimate the relative permeability curves, the capillary pressure curve, and the longitudinal dispersion coefficient.

1. INTRODUCTION

Immiscible and miscible displacement experiments are commonly used to determine the two-phase flow and hydrodynamic dispersion coefficients of soils, respectively. The capillary pressure and relative permeability curves may be determined by performing either steady-state experiments with the simultaneous flow of two fluids through the porous medium (Avraam and Payatakes, 1995) or transient experiments of the displacement of the one fluid by the other (Chen et al., 1999). The hydrodynamic dispersion coefficients are estimated from miscible displacement experiments by fitting analytic or numerical solutions of the advection-dispersion equation to the temporal evolution of the solute concentration at various axial positions along the porous medium (Sahimi, 1995; Tsakiroglou et al., 2005).

In a steady-state immiscible displacement experiment, simultaneous injection of both fluids through the porous medium is accomplished by keeping constant the flow rate of the one fluid and varying the flow rate of the other one, until equilibrium is established (Avraam and Payatakes, 1995). In unsteady-state methods the measured transient responses of the fluid saturation and pressure drop across the porous medium are introduced into inverse modeling solvers of the macroscopic two-phase flow equations to estimate the capillary pressure and relative permeability curves (Sigmund and McCaffery, 1979; Mitlin et al., 1999; Toth et al., 2002; Tsakiroglou et al., 2003, 2005).

The miscible displacement involves two fluids that mix in all proportions, and their mixture remains a single phase (Sahimi, 1995). The variation of the dispersion coefficient with the Peclet number has extensively been investigated by using a variety of techniques (acoustic, NMR, CT-Scan, radioactive tracers, color tracers, etc) to measure the transient changes of the spatial distribution of the solute concentration over the porous medium (Ding and Candela, 1996; Peters et al., 1996; Drazer et al., 1999; Manz et al., 1999; Tsakiroglou et al., 2005).

The goal of the present work is to (a) develop a new method for the simultaneous determination of the multiphase effective transport coefficients of disturbed soils by monitoring multi-point measurements of the electrical resistance during transient immiscible and miscible displacement experiments, and (b) correlate the so-measured transport properties with heterogeneities of the pore space. To this scope, an in-house constructed multipoint conductivity meter is used to measure the electrical transient response of the resistance between vertical ring electrodes and horizontal rod electrodes that have properly been assembled to the soil holder. The electrical measurements are converted to transient responses of water saturation and solute concentration. Numerical codes of inverse modeling of the two-phase flow and advection-dispersion equations are employed to estimate the capillary pressure curve, relative permeability curves, and longitudinal dispersion coefficient for two sandy soils characterized by narrow and broad grain size distribution, respectively.

2. MATERIALS AND METHODS

An experimental apparatus was constructed to measure the electrical conductance of disturbed soils during immiscible and miscible displacement experiments. The apparatus consists of a PTFE holder equipped with two end electrodes and intermediate ring electrodes, an in–house constructed multi-point conductivity meter, a HPLC pump, a weight balance and a differential pressure transducer (Fig.1a). All experimental data are transmitted to a data acquisition card installed in the host computer. The total length of the soil column is L=30 cm and the diameter D=5 cm.

Two soil samples were tested: (1) a well-sorted commercial sand (S1) with narrow grain size distribution (D_g=125-250 μm), porosity ϕ=0.40 and permeability k=35.8 Da; (2) a sandy soil (S2) collected from North Poland (Kluczewo airport) with broad grain size distribution (D_g=50-1400 μm), porosity ϕ=0.36 and permeability k=21.8 Da. The soil sample S2 was cleaned carefully by treating it with ethanol, methanol and toluene and then was sieved to remove the silt (grains of diameter<50 μm).

Initially the porous medium is fully saturated with the wetting fluid (aqueous solution of NaCl 0.5% w/v). Multi-step immiscible displacement experiments were performed by injecting n-dodecane through the porous medium with the HPLC pump at a constant flow rate (q=0.2 ml/min) until equilibrium conditions are established. Afterwards, the flow rate increases (q=1.0 ml/min-q=3.0 ml/min) and the electrical conductivity across five segments of the sand column (Fig.1b), the effluent weight, and the total pressure drop across the soil column were monitored until a new steady-state was reached and so forth.

During a miscible displacement experiment, the porous medium was initially fully saturated with a low NaCl concentration solution (C_0 =17.1 mol/m^3) and then, the high NaCl concentration solution (C_i =68.4 mol/m^3) was injected at a constant flow rate upwards in order to avoid a destabilized displacement pattern. The transient response of the electrical resistance between horizontal electrodes (Fig.1c) on selected cross sections of the soil column was measured and the conductivities were transformed to solute concentration breakthrough curves with the aid of calibration curves constructed from standard solutions.

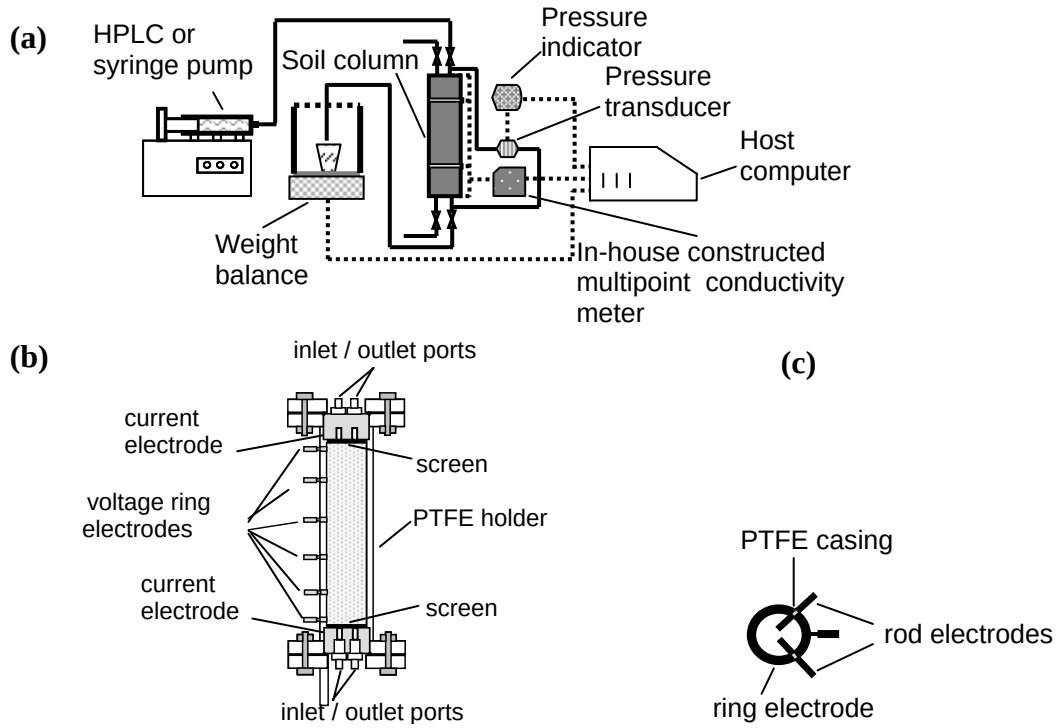

FIGURE 1. (a) Setup for performing immiscible displacement experiments. (b) Schematic diagram of resistivity cell. (c) Overview of rod electrodes.

3. DATA PROCESSING AND INVERSE MODELING

3.1 Determination of water saturation profiles from electrical resistivity

The capillary number Ca is defined by

$$Ca = \frac{q_o \mu_o}{A \gamma_{ow}} \tag{1}$$

where q_o is the oil flow rate, A is the total cross-sectional area, μ_o is the oil viscosity and γ_{ow} is the oil/water interfacial tension. Results of a multi-step immiscible displacement experiment performed on soil S2 at capillary numbers Ca =9.7x10^{-8}, Ca =4.85x10^{-7} and Ca =1.45x10^{-6} are shown in Fig.2. The electrical resistance is measured in five soil segments between the reference upper electrode 1 and five lower electrodes (1-2, 1-3, 1-4, 1-5, 1-6)

(Fig.1b). Up to the point that oil reaches the lower electrode, the water saturation of each segment is calculated easily from the volume injected and the weight of the effluents. Then, the resistivity index and water saturation values for each cumulative soil segment are fitted to the model (Aggelopoulos et al., 2005)

$$I_R = \left[a S_w{}^m + (1-a) S_w{}^l \right]^{-1} \tag{2}$$

for estimating the parameters a, m and n. Eq.(2) is extrapolated to lower water saturations by transforming the measured resistivity index of each cumulative segment to water saturation. With the aid of simple mass balances of the form

$$S_{w1-3} = \left(S_{w1-2} V_{p12} + S_{w2-3} V_{p23} \right) / V_{13} \tag{3}$$

the water saturation (S_{w1-2}, S_{w2-3}, S_{w3-4}, S_{w4-5}, S_{w5-6}) of each differential soil segment is obtained (Fig.2b). At steady-state, the axial distribution of water saturation along the soil column is not uniform but increases in the deeper layers (Fig.2b). This is due to the capillary end effect, associated with the discontinuity of the capillary pressure at the outlet of the porous medium (Huang and Honarpour, 1998; Toth et al., 2002).

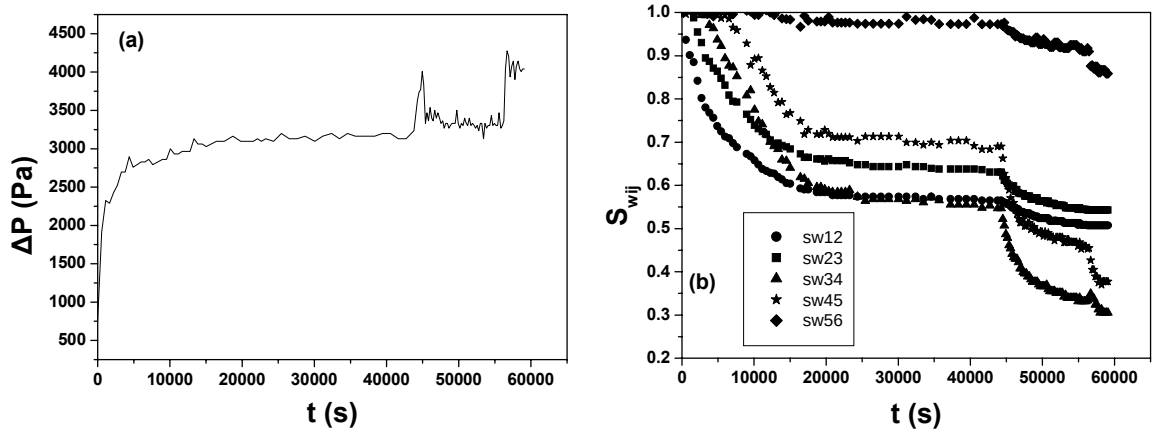

FIGURE 2. (a) Transient response of the pressure drop across the column (soil S2).
(b) Transient response of the water saturation in the column segments 1-2, 2-3, 3-4, 4-5, 5-6 (soil S2).

3.2 History matching of immiscible displacement datasets and parameter estimation

In a homogeneous and isotropic porous medium of permeability k and porosity φ, the one-dimensional immiscible displacement of a wetting aqueous phase (w) by a non-wetting oil (o) is described by the following averaged mass and momentum balances (Sahimi, 1995)

$$\phi \frac{\partial S_o}{\partial t} + \frac{\partial u_o}{\partial x} = 0 \qquad \phi \frac{\partial S_w}{\partial t} + \frac{\partial u_w}{\partial x} = 0 \tag{4}$$

$$u_o = \frac{k k_{ro}}{\mu_o} \left(- \frac{\partial P_o}{\partial x} \right) \qquad u_w = \frac{k k_{rw}}{\mu_w} \left(- \frac{\partial P_w}{\partial x} \right), \tag{5}$$

where $S_j, P_j, u_j, k_{rj}, \mu_j$ ($j = w, o$) are the saturation, pressure, superficial velocity, relative permeability, and viscosity of the phase j. The capillary pressure $P_c = P_o - P_w$ and relative permeability curves k_{rw}, k_{ro} are represented by the following Corey type functions:

$$P_c = P_c^0 \left(1 - \frac{S_o}{1 - S_{wi}} + b_c \right)^{-m_c}, \tag{6}$$

$$k_{rw} = k_{rw}^0 \left(1 - \frac{S_o}{1 - S_{wi}} + b_w \right)^{m_w} \left(\frac{1}{1 + b_w} \right)^{m_w}, \tag{7}$$

$$k_{ro} = k_{ro}^0 \left(\frac{S_o}{1 - S_{wi}} + b_{nw} \right)^{m_{nw}} \left(\frac{1}{1 + b_{nw}} \right)^{m_{nw}}. \tag{8}$$

The measured transient responses of $\Delta P(t)$ and $S_{wi-j}(t)$ are introduced into a numerical solver of the aforementioned macroscopic two-phase flow equations to estimate the parameters of the capillary pressure and relative permeability curves, Eqs.(6)-(8). The $k_{rw}(S_o), k_{ro}(S_o), P_c(S_o)$ are so selected that the numerically calculated responses of $\Delta P(t)$ and $S_{wi-j}(t)$ fit to the corresponding experimental measurements. The inverse modeling was done in the environment of Athena software package by using the Bayesian estimator of the Gregplus solver (Tsakiroglou et al., 2003, 2005), and the results are shown in Fig.3

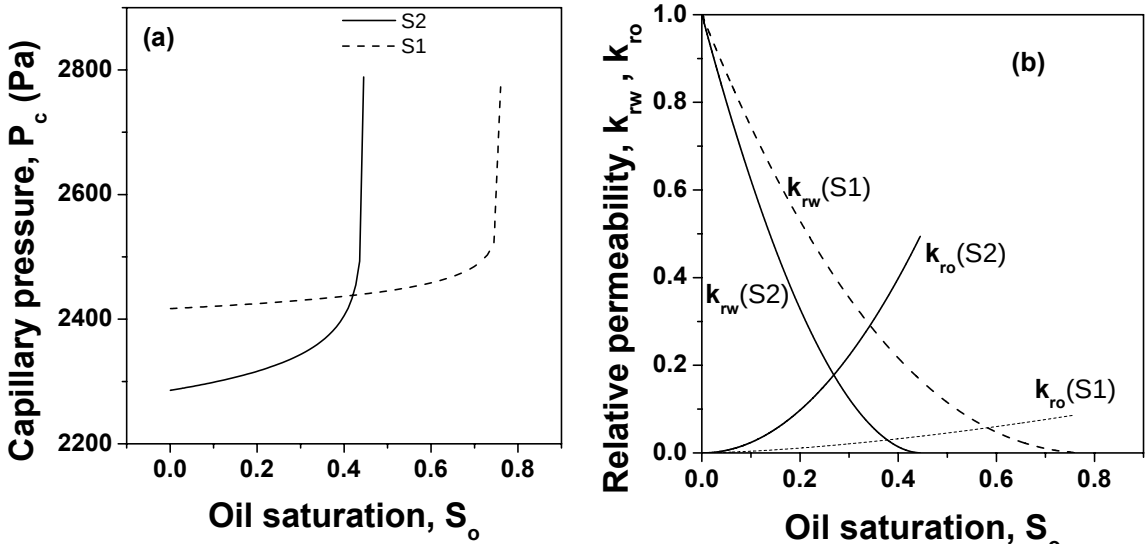

FIGURE 3. (a) Estimated capillary pressure curves. (b) Estimated water and oil relative permeability curves.

The $P_c(S_o)$ of soil S2 is wider than that of soil S1 whereas the entry pressure [$P_c(S_o = 0)$] of S2 is lower than that of soil S1 (Fig.3a). It is well known that, at vanishing flow rates, the pore-throat size distribution is reflected in the position and width of $P_c(S_o)$ (Tsakiroglou and Payatakes, 1990). Because of the broad grain size distribution, the throat size distribution of S2 is much wider than that of sample S1 (narrow grain size distribution) with result that oil

invasion starts at lower capillary pressures and is completed over a wider pressure range compared to sample S1. The high value of the irreducible water saturation (S_{wi} =0.555) can be attributed to the broad pore size distribution of the soil S2. According to percolation theory, the invasion of a non-wetting fluid (oil) in a pore system with a broad pore size distribution follows the most permeable highways of the percolation cluster (Sahimi, 1995). Moreover, the hydraulic conductivity (absolute permeability) of such a system is also dominated by the conductivity of a critical path, a subset of which is the percolation cluster (Tsakiroglou, 2002). Therefore, for soil S2, the effective permeability of the injected non-wetting fluid at the irreducible wetting fluid saturation ($S_o = 1 - S_{wi}$) is not expected to be distant from the absolute permeability of the porous medium, and for this reason, the end oil relative permeability is high enough (Fig.3b).

3.3 Estimation of the longitudinal hydrodynamic dispersion coefficient

Miscible displacement experiments of a low NaCl concentration solution by a high NaCl concentration solution were performed on the sandy soils S1 and S2 at varying values of the Peclet number defined by

$$Pe = u_p \langle D_g \rangle / D_m \tag{9}$$

where $u_p = q/(\phi A)$ is the pore velocity, ϕ is the porosity, $\langle D_g \rangle$ is the mean grain diameter, and D_m is the NaCl-H_2O bulk diffusion coefficient ($D_m = 1.6x10^{-9}$ m^2/s). For the soil S1 (ϕ=0.4, $\langle D_g \rangle$=200 μm) the solute concentration breakthrough curves were measured at two distances from the column inlet as it is shown in Fig.4a. The experimental data were fitted to the analytic solution of the one-dimensional advection-dispersion equation given by

$$C^* = \frac{C - C_i}{C_0 - C_i} = \frac{1}{\sqrt{\pi}} \int_{\beta}^{\infty} \exp\left(-\kappa^2\right) d\kappa + \frac{1}{\sqrt{\pi}} \exp\left(\frac{x u_p}{D_L}\right) \int_{a}^{\infty} \exp\left(-\kappa^2\right) d\kappa \tag{10}$$

where

$$\beta = \frac{x - u_p t}{2(D_L t)^{1/2}} \qquad \alpha = \frac{x + u_p t}{2(D_L t)^{1/2}} \tag{11}$$

The Bayesian estimator of Athena software package was employed to estimate simultaneously the mean pore velocity, $u_{p,est}$ (Fig.4c) and longitudinal dispersion coefficient, D_L (Fig.4b). The estimated pore velocity, $u_{p,est}$, is very close to that calculated from the current flow rate and porosity (Fig.4c), whereas the estimated dispersion coefficient, D_L/D_m (Fig.4b) is in full agreement with corresponding data of literature (Sahimi, 1995). The variation of the longitudinal dispersion coefficient with the Peclet number follows power laws with an exponent tending to 1 or 2, depending on whether macrodispersion (associated with the spatial variation of the pore sizes) or Taylor dispersion (associated with the flow channeling within individual pores) is the dominant dispersion mechanism (Fig.4b).

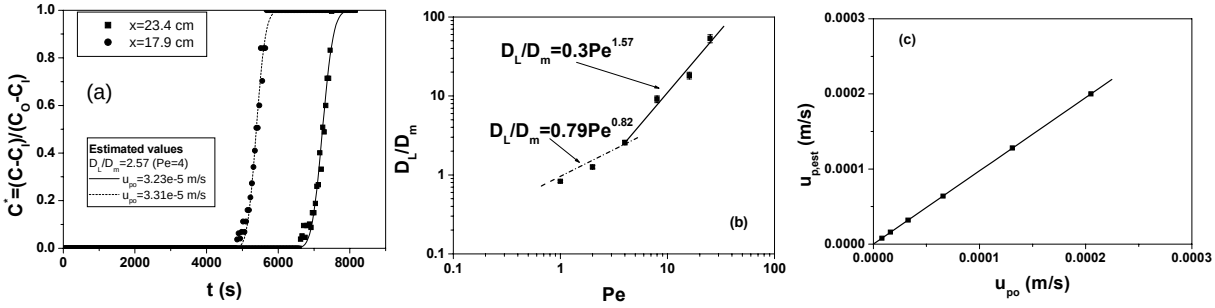

FIGURE 4. (a) Experimentally measured vs numerically predicted solute concentration breakthrough curves (S1). (b) Longitudinal dispersion coefficient (S1). (c) Estimated pore flow velocity vs mean pore velocity (S1).

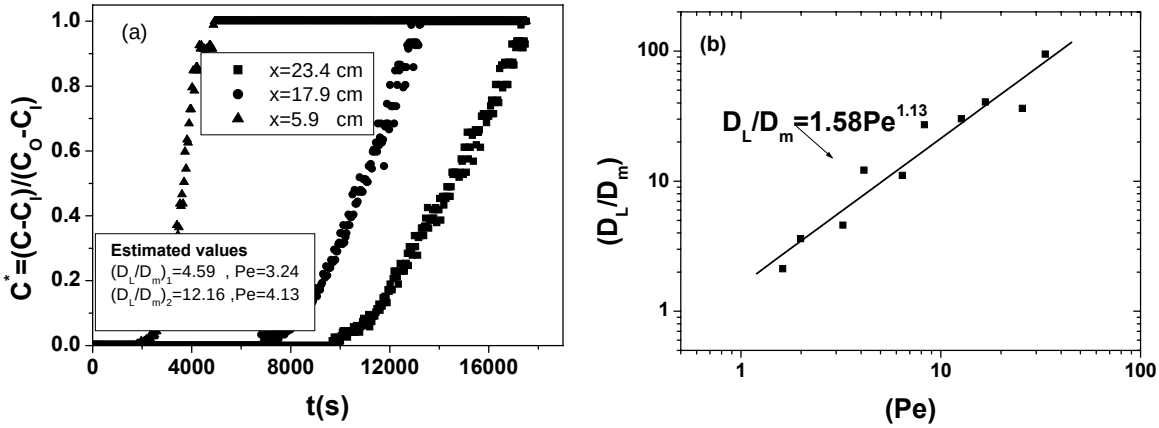

FIGURE 5. (a) Experimentally measured solute concentration breakthrough curves (S2). (b) Longitudinal dispersion coefficient (S2).

For the soil S2 (ϕ=0.36, $\langle D_g \rangle$=350 μm) the solute concentration breakthrough curves were measured at three distances from the column inlet as shown in Fig.5a. These curves are consistent with solute breakthrough curves obtained for dual porosity media. In such a case, the pore velocity varies significantly across a cross-sectional area, solute molecules prefer to move along the high velocity streamlines of the large pores whereas pore regions dominated by low flow velocities are bypassed. This process was modeled as a convective-dispersive process controlled by two dispersion coefficients and two pore velocities (one for the system of large pores and another for the system of small pores). A dimensionless concentration C_j^* ($j=1,2$) is derived from Eq.(10) for each pair of parameters (D_{lj}, u_{pj}). However, the measured solute concentration at each axial position of the soil column can be regarded as a concentration averaged over the entire cross-section and can be related to the other two concentrations through a solute flux balance of the form

$$C^* = \left(u_{p1}C_1^* + u_{p2}C_2^*\right)\Big/ u_p \tag{12}$$

where the mean pore velocity is given by

$$u_p = f u_{p1} + (1-f)u_{p2} \tag{13}$$

and f, $1-f$ are the contribution fractions of the two porosities to the total flow. In this

manner, D_{L1} , D_{L2}, $u_{p1,est}$, $u_{p,est}$ were estimated simultaneously. From the estimated pore velocities the corresponding Peclet numbers were calculated through Eq.(9) and the results are shown in Fig.5b. The variation of the longitudinal dispersion coefficient with the Peclet number follows a power law with an exponent equal to 1.13 which indicates that macrodispersion is the dominant dispersion mechanism over the entire range of Pe values.

ACKNOWLEDGEMENTS

This work was performed under Global Change and Ecosystems contract number SSPI-CT-2003-004017-STRESOIL (2004-2007) supported by the European Commission.

REFERENCES

1. Aggelopoulos, C., P. Klepetsanis, M. Theodoropoulou, K. Pomoni, and C.D. Tsakiroglou (2005), Large-scale effects on the resistivity index of porous media, *J. Contam. Hydrology, 77***,** 299-323.
2. Avraam, D.G. and A.C. Payatakes (1995), Flow regimes and relative permeabilities during steady-state two-phase flow in porous media, *J. Fluid Mech., 293*, 207-236.
3. Chen, J., J.W. Hopmans, and M.E. Grismer (1999), Parameter estimation of two-fluid capillary pressure-saturation and permeability functions, *Adv. Water Resour., 22*, 479-493.
4. Ding, A., and D. Candela (1996), Probing non-local tracer dispersion in flows through porous media, *Phys. Rev. E, 54*, 656-660.
5. Drazer, G., R. Chertcoff, L. Bruno, M. Rosen, and J. P. Hulin (1999), Tracer dispersion in packings of porous activated carbon grains, *Chem. Eng. Sci., 54*, 4137-4144.
6. Huang, D.D. and M.M. Honarpour (1998), Capillary end effects in coreflood calculations, *J. Pet. Sci. Eng.*, *19*, 103-117.
7. Inoue, M., J. Simunek, S. Shiozawa, J.W. Hopmans (2000), Simultaneous estimation of soil hydraulic and solute transport parameters from transient infiltration experiments, *Adv. Water Resour.*, *23*, 677-688.
8. Manz, B., P. Alexander, and L. F. Gladen (1999), Correlations between dispersion and structure in porous media probed by nuclear magnetic resonance, *Phys. Fluids*, *11*, 259-267.
9. Mitlin, V., B. Lawton, and L. Owen (1999), A semi-analytical procedure for estimating relative permeability from displacement experiments: Account for pre-breakthrough data, *Int. J. Eng. Sci., 37*, 1051-1067.
10. Peters, E. J., R. Gharbi, and N. Afzal (1996), A look at dispersion in porous media through computed tomography imaging, *J. Pet. Sci. Eng.*, 15, 23-31.
11. Sahimi M. (1995), *Flow and Transport in Porous Media and Fractured Rock***:** *From Classical Methods to Modern Approaches*, VCH, Weinheim, Germany.
12. Sigmund, P., and F. McCaffery (1979), An improved unsteady-state procedure for determining the relative permeability characteristics of heterogeneous media, *SPE J., 169*, 15-28.
13. Toth, J., T. Bodi, P. Szucs and F. Civan (2002), Convenient formulae for determination of relative permeability from unsteady-state fluid displacements in core plugs, *J. Pet. Sci. Eng., 36*, 33-44.
14. Tsakiroglou, C.D. (2002), Determination of the transport properties of single fractures with the aid of critical path analysis, *Ind. Eng. Chem. Res., 41*, 3462-3472.
15. Tsakiroglou, C. D and A. C. Payatakes (1990), A new simulator of mercury porosimetry for the characterization of porous materials, *J. Colloid Interface Sci., 137*, 315-339.
16. Tsakiroglou, C.D., M. Theodoropoulou, and V. Karoutsos (2003), Non-equilibrium capillary pressure and relative permeability curves of porous media, *AIChE J., 49***,** 2472-2486.
17. Tsakiroglou, C.D., M.A. Theodoropoulou, V. Karoutsos, and D. Papanicolaou (2005), Determination of the effective transport coefficients of pore networks from transient immiscible and miscible displacement experiments, *Water Resources Research, 41(2)*, W02014.